

Exploiting diurnal temperature variations to monitor the growth of tubers

Bezemer, Marissa; Budko, Neil

10.1186/s13362-025-00178-9

Publication date

Document Version Final published version

Published in Journal of Mathematics in Industry

Citation (APA)

Bezemer, M., & Budko, N. (2025). Exploiting diurnal temperature variations to monitor the growth of tubers. Journal of Mathematics in Industry, 15(1), Article 13. https://doi.org/10.1186/s13362-025-00178-9

Important note

To cite this publication, please use the final published version (if applicable). Please check the document version above.

Other than for strictly personal use, it is not permitted to download, forward or distribute the text or part of it, without the consent of the author(s) and/or copyright holder(s), unless the work is under an open content license such as Creative Commons.

Takedown policy

Please contact us and provide details if you believe this document breaches copyrights. We will remove access to the work immediately and investigate your claim.

RESEARCH Open Access



Exploiting diurnal temperature variations to monitor the growth of tubers

Marissa Bezemer^{1,2} and Neil Budko^{1*}

*Correspondence: n.v.budko@tudelft.nl

¹Numerical Analysis, Delft Institute of Applied Mathematics, Faculty of Electrical Engineering, Mathematics and Computer Science, Delft University of Technology, Mekelweg 4, 2628 CD Delft, The Netherlands Full list of author information is available at the end of the article

Abstract

We propose to use diurnal temperature variations for nondestructive monitoring of growing tubers and investigate the feasibility by numerically simulating the data collected with a grid of passive thermal sensors placed in the ground and sampled at regular time intervals. A qualitative linear imaging algorithm that produces an approximate projected view of the tubers is proposed and an effective inversion method is applied to recover the volume fraction of tubers. In particular, it is shown that a correlation-based cost functional outperforms the usual least-squares metric, although, requiring additional steps to deal with the non-uniqueness of the solution.

Keywords: Inverse problems; Agriculture; Subsurface imaging

1 Introduction

Phenotyping and yield prediction of tuberous and root crops such as potato, cassava and yam require digging up, analyzing and discarding numerous plants at various times during the season, which is time-consuming, laborious, destructive and wasteful. Attempts to adapt existing non-destructive subsurface imaging techniques, such as ground penetrating radar [1], face obvious difficulties due to the above-ground leaves and branches that deny direct access to the soil surface. If antennas are to be placed above the plants, then one can expect significant reflection and distortion of probing electromagnetic and acoustic signals, which can not be removed by simple subtraction as canopies grow and change with time.

Natural diurnal air temperature variations create temperature "waves" that slowly propagate into the subsurface and rapidly decay with depth [2]. Similar to the electromagnetic waves of the ground-penetrating radar, these temperature waves are distorted by the tubers, e.g., potatoes. The thermal contrast of tubers with respect to a typical soil is high enough even in wet circumstances due to the difference in heat capacity. Therefore a question emerges whether these natural temperature waves can be exploited to visualize and measure the state of tubers at any given time, in particular, their number, size, shape and location. Since temperature waves decay very rapidly, it is clear that sensors must be placed sufficiently close to both the ground surface and the tubers. Where exactly should these sensors be placed, what should be their sensitivity and sampling rate are some of the open questions addressed in this paper. Previously, artificially excited thermal waves



© The Author(s) 2025. **Open Access** This article is licensed under a Creative Commons Attribution 4.0 International License, which permits use, sharing, adaptation, distribution and reproduction in any medium or format, as long as you give appropriate credit to the original author(s) and the source, provide a link to the Creative Commons licence, and indicate if changes were made. The images or other third party material in this article are included in the article's Creative Commons licence, unless indicated otherwise in a credit line to the material. If material is not included in the article's Creative Commons licence and your intended use is not permitted by statutory regulation or exceeds the permitted use, you will need to obtain permission directly from the copyright holder. To view a copy of this licence, visit http://creativecommons.org/licenses/by/4.0/.

Table 1 Material parameters

	k, W/(m K)	$ ho$, kg/m 3	<i>C_p</i> , J/(kg K)
Soil	0.3	1300	800
Potato	0.56	1079	4036

have successfully been applied for imaging of inhomogeneous solids [3, 4]. Natural diurnal temperature waves, however, do not have a broad spectrum and may require a different approach.

In the following sections realistic three-dimensional heat transfer simulations are employed to determine the characteristic temperature ranges and estimate the required spatial/temporal resolution and sensitivity of temperature sensors. A simple imaging algorithm is proposed to visualize the lateral distribution of tubers and an effective inversion method is applied to nondestructively determine the tubers state over the season.

2 Modeling

The temperature distribution $T(\mathbf{x},t)$ in the configuration depicted in Fig. 1 (left) is assumed to satisfy the following heat transfer problem:

$$\rho C_{p} \frac{\partial T}{\partial t} - \nabla \cdot (k \nabla T) = 0, \quad \mathbf{x} \in \Omega, \quad t \in (0, t_{\text{end}}];$$

$$T(\mathbf{x}, 0) = T_{\text{amb}}(0), \quad \mathbf{x} \in \Omega;$$

$$\mathbf{n} \cdot (k \nabla T) = \epsilon \sigma (T_{\text{amb}}^{4} - T^{4}), \quad \mathbf{x} \in \partial \Omega_{\text{top}};$$

$$\mathbf{n} \cdot (k \nabla T) = 0, \quad \mathbf{x} \in \partial \Omega_{\text{bottom}};$$

$$\mathbf{n}_{1} \cdot (k_{1} \nabla T_{1}) = -\mathbf{n}_{2} \cdot (k_{2} \nabla T_{2}); \quad T_{1} = T_{2}, \quad \mathbf{x} \in \partial \Omega_{\text{sides}},$$
(1)

where the last boundary condition is periodic. The values of the material parameters for soil and potatoes [5–7] have been set as in Table 1 and the surface emmissivity was set as $\epsilon=0.92$ and the simulation time as $t_{\rm end}=192$ h. The ambient air temperature $T_{\rm amb}(t)$ was extracted from historical meteorological data for the period starting on June 1, 2016, in Leeuwarden (Netherlands).

Geometry of the problem mimics a typical "ridge" structure where the seed potato is planted in the center of an elevated ridge at the depth of 12.5 cm from the surface and the new potatoes of different sizes and shapes emerge later at approximately the same average depth and tend to remain within the ridge. Three stages in the growth of new potatoes depicted as horizontal projections of Fig. 4 (top) have been modelled. Numerical solution of the heat transfer problem (1) was obtained with the Finite Element Method (FEM) in the Comsol Multiphysics 5.4 software package.

A snapshot of the resulting temperature wave can be seen in Fig. 1 (right), where on the soil surface the temperature has already reached its daily maximum (red color), whereas the minimum of the preceding night (blue color) is still propagating downwards into the subsurface. It is also clear that the wave diminishes very rapidly with depth as no discernible temperature variations can be seen below the first wave cycle. Nonetheless, it is also clear that the first wave cycle covers the typical potato depths (down to 40 cm).

Figure 2 shows temperature variations at several points in the configuration. Namely, T_1 is at the surface above an empty (no potatoes) spot, T_2 is exactly below the location of

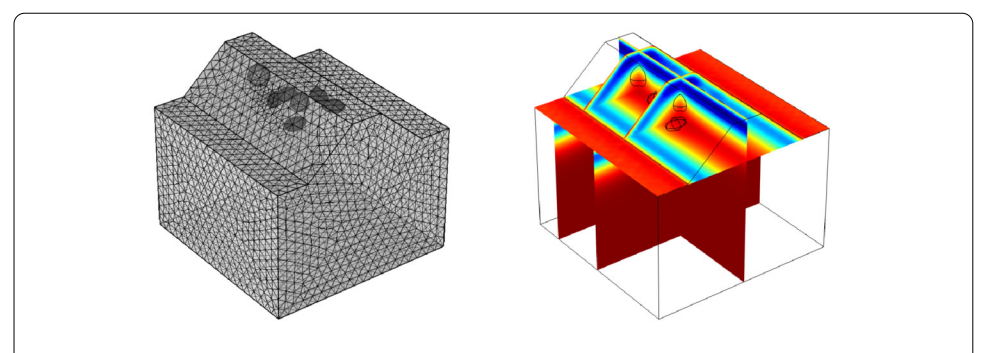


Figure 1 Three-dimensional configuration with the generated mesh (left) and the computed temperature distribution snapshot showing the subsurface temperature wave (right)

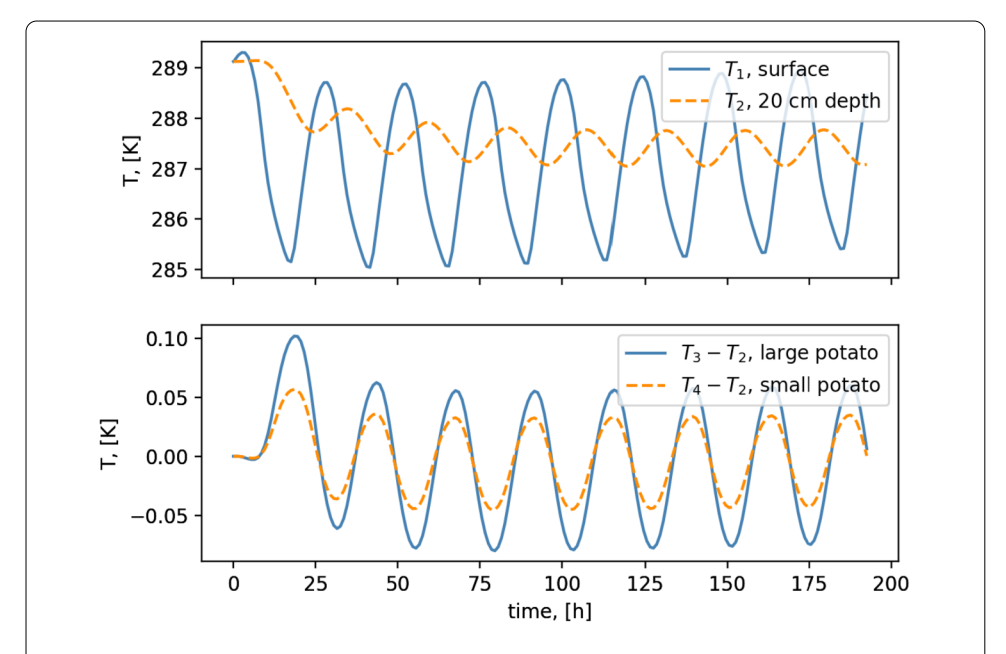


Figure 2 Top: temperature without potatoes as a function of time; T_1 – at the surface, T_2 – at 20 cm depth. Bottom: temperature difference at 20 cm due to the presence of large and small potatoes (spheres of 10 cm and 8 cm diameters with centers at 12.5 cm depth). Initial parts of the plots (up to 75 hours) correspond to the transient period in simulations

 T_1 , but at 20 cm depth, T_3 and T_4 are the temperatures measured at 20 cm depths below a large (10 cm diameter) and small (8 cm diameter) potatoes, respectively. Note that the bottom plot of Fig. 2 shows the differences $T_3 - T_2$ and $T_4 - T_2$. The transient period up to 75 h is an artefact of the wrong initial condition $T(\mathbf{x},0) = T_{\rm amb}(0)$ and should be disregarded. The top plot of Fig. 2 shows an oscillating signal in time, typical for a quasi-harmonic wave, that diminishes in amplitude with depth and undergoes a phase shift. The amplitude of variations reduces from approximately 4 degrees at the surface to just one degree at 20 cm depth. As can be seen in the bottom plot of Fig. 2, the influence of potatoes on the signal at 20 cm are in the order of 0.1 degrees. This means that, if one would like to detect potatoes, then the amplitude resolution should be at least 0.01 degrees. It is well-known that achieving 0.01 degree absolute accuracy in temperature measurements is a very difficult task. Therefore, any viable imaging or inversion algorithm should rely on the

relative stability and high (amplitude) resolution of the measurements rather than absolute accuracy.

In particular, a relative calibration procedure of temperature sensors should be implemented. For example, if the data are to be collected by a horizontal wire-mesh of thermistors, then all thermistors should be (numerically) calibrated to give the same readings and slopes in an environment with controlled spatially uniform temperature. The high-frequency electronic noise should not be a problem as the data may be collected at hourly intervals, leaving enough time for signal averaging.

3 Imaging

Comparing the top plot (blue, solid curve) with the curves in the bottom plot of Fig. 2 one can notice the expected phase shift between the background temperature and the temperature-difference signals. A very basic imaging algorithm can be applied to convert this local phase shift into a two-dimensional image of potatoes.

Let the input data be collected over a doubly uniform grid $\{(x_i, y_j) | i = 1, ..., 20; j = 1, ..., 20\}$ with 2 cm spatial step located at 20 cm depth, approximately covering the base of the ridge. Specifically, assuming discrete data measured at 1-hour intervals $T(x_i, y_j, t_m)$, m = 1, ..., M; and the corresponding background temperature $T_b(x_i, y_j, t_m)$, m = 1, ..., M; measured at the same depth in an area free from potatoes, the image $I(x_i, y_j, t_M)$, can be computed as follows:

$$I(x, y, t_M) = L(x, y) \left[\sum_{m=1}^{M} \left[T(x_i, y_j, t_m) - T_b(x_i, y_j, t_m) \right] T_b(x_i, y_j, t_m) \right], \tag{2}$$

where L(x, y) denotes the interpolation operator for locations (x, y) that fall between the grid points (x_i, y_j) . Images obtained with different choices of t_M are shown in Fig. 3, and the 24-hour interval consisting of M = 25 time samples per sensor and containing the full temperature-wave cycle appears to provide the best contrast.

The phase shift of the temperature-difference signals with respect to the background signal results in locally negative values of the function $I(x, y, t_M)$. This negative contrast is, however, not uniquely determined by the size of tubers alone and is also influenced by potato's proximity to the measurement plane. The relatively good lateral resolution of the images stems from the exponential decay of temperature perturbations away from their origin, i.e., tubers, in the present case. At the same time this exponential decay leads to the "disappearance" of potatoes situated too far away from the measurement plane. This is a well-known drawback of all imaging algorithms based on diffusive fields [3, 4]. Nevertheless, one can easily detect the presence of at least five (out of six) tubers in the images of Fig's 3-4.

Despite the difficulty in interpreting the images the algorithm is sensitive enough to capture the emergence and growth of new potatoes as illustrated in Fig. 4. The noise in the first image is of numerical origin due to a relatively rough FEM mesh and very weak temperature-difference signals produced by the 2 cm potato tubers. The colorbars show that the negative contrast increases with the size of tubers. Note that the surfaces of growing tubers move closer to the detector plane as well.

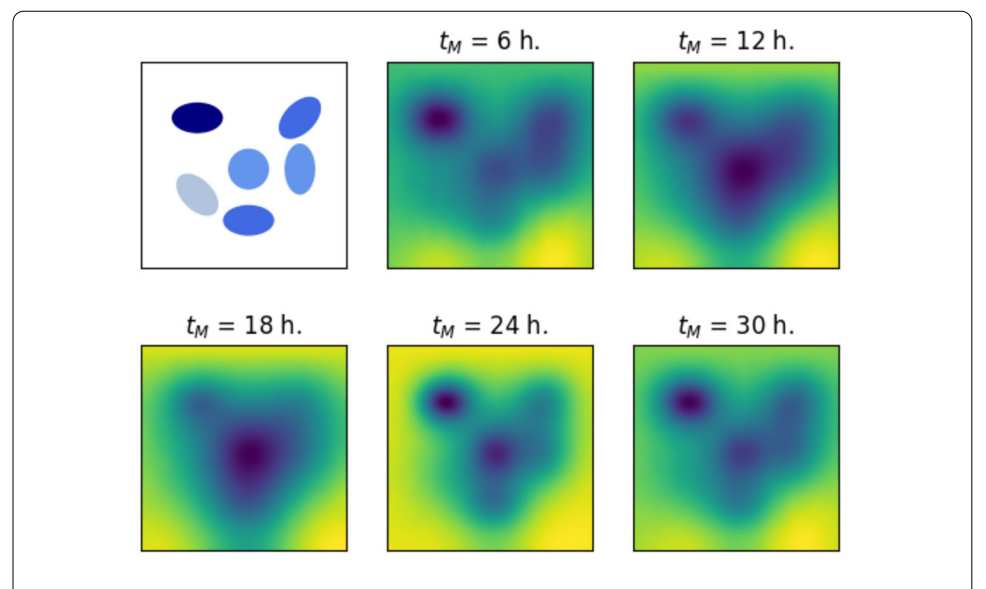
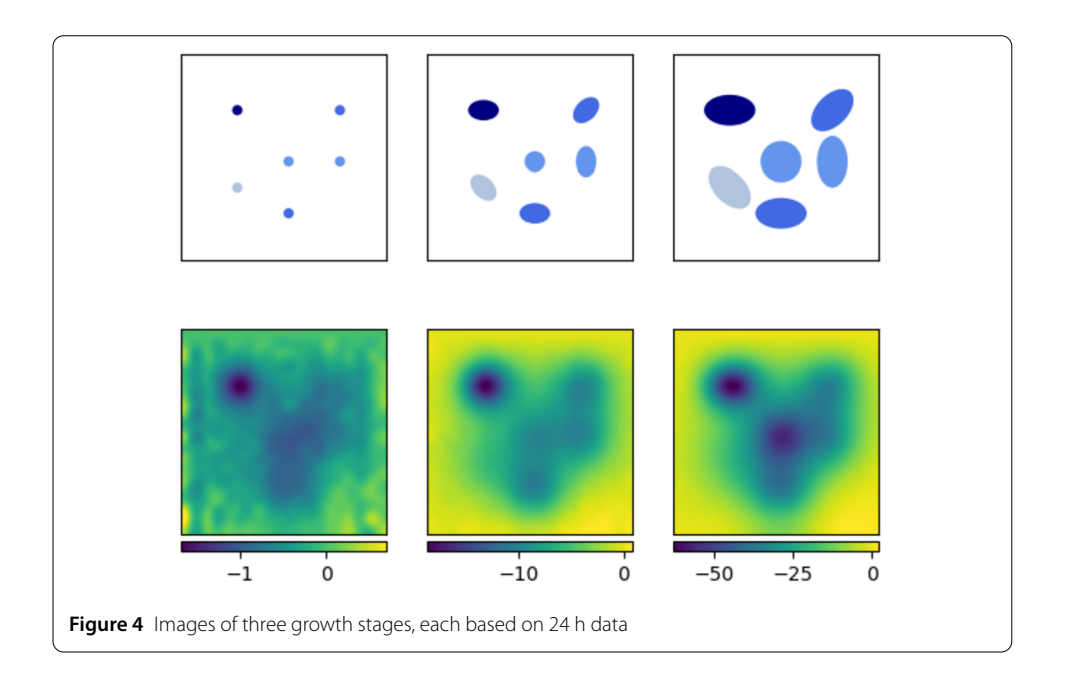


Figure 3 Top-left: horizontal two-dimensional projection (shadows) of 6 potatoes (see Fig. 1) with color coding indicating the distance from the measurement plane (dark means close). Rest: Images $I(x, y, t_M)$ obtained with Eq. (2) for different t_M



4 Effective inversion

Another approach that works with limited and noisy data is called *effective inversion* [8–10]. The basic idea is to fit the data with an easy to interpret low-dimensional model that captures the essence of the object-data relation. When dealing with inhomogeneous targets, such as a group of tubers, the effective model is typically homogeneous and covers the domain where one expects the tubers to be present. The material parameter of this homogeneous model, thermal diffusivity $D = k/(\rho C_p)$, that produces the best fit to the measured data is denoted as $D_{\rm eff}$ and is called the *effective* diffusivity.

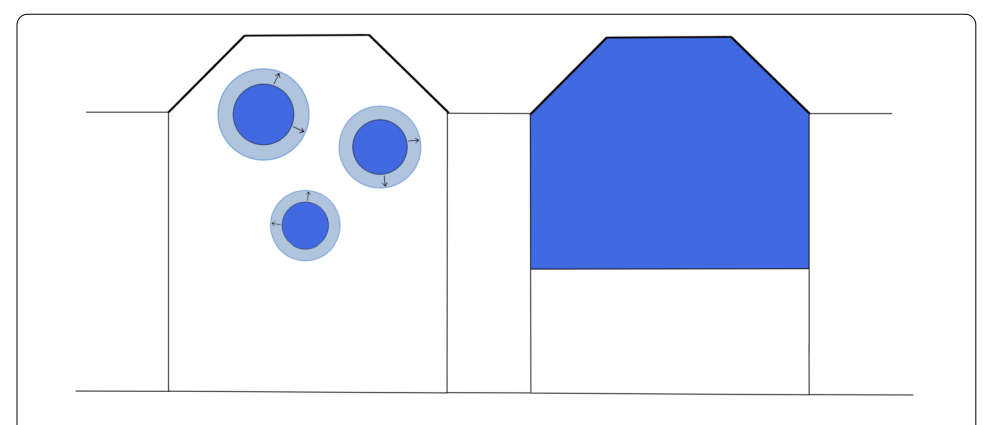


Figure 5 Schematics of the original (left) and effective (right) two-dimensional models. The growing potatoes are modelled as the time varying diffusivity of a homogeneous effective domain

The actual thermal diffusivities of soil and potatoes assumed here, see Table 1, are $D_{\rm s} = 2.88 \times 10^{-7} \, {\rm m^2/s}$ and $D_{\rm p} = 1.29 \times 10^{-7} \, {\rm m^2/s}$, respectively. Hence, the effective diffusivity of the homogeneous model is expected to be somewhere between these values, depending on the amount and sizes of potatoes within the effective domain. During the season, as potatoes emerge and grow, the effective diffusivity $D_{\rm eff}$ will start off as $D_{\rm s}$ and then gradually approach a smaller value closer to $D_{\rm p}$, thus indicating the amount and the rate of growth of potatoes.

Numerical experiments in this Section have been performed on the two-dimensional configuration depicted in Fig. 5. The growth of potatoes is modelled on a fine temporal scale with the radius of each tuber increasing at the rate of 0.86 mm/day, reaching the final radius of 6 cm at the end of the 70-day season. The boundary conditions and material parameters are the same as in Eq. (1) and Table 1 with the exception of emissivity, which was set to $\epsilon = 0.8$. The corresponding heat transfer problem is solved numerically with the Finite-Element Method using the Fenics (dolfin) module in Python. There are 12 randomly placed potatoes in the particular numerical experiments presented below.

Let $T(x_i, t_m)$ be the simulated data generated by the forward heat transfer model of growing potatoes with diffusivity D_p , where x_i , $i=1,\ldots,N$, are the locations of thermal detectors uniformly placed at 1 cm intervals along a horizontal 60 cm line segment situated 45 cm below the top of the ridge. We denote as $T_{\rm eff}(x_i,t_m,D)$ the temperature that would have been measured at the same locations and at the same times if instead of potatoes there would be a homogeneous block with diffusivity D as shown in Fig. 5 (right). The diffusivity of the soil D_s , the ambient temperature $T_a(t)$, and the background (no potatoes) temperature $T_b(x_i,t_m)$ at the detector line are considered to be known and the same in both models. The goal is to match the data $T(x_i,t_m)$ and the temperature $T_{\rm eff}(x_i,t_m,D)$ by tuning the diffusivity D of the effective model. The value of D that provides the best match is the effective diffusivity will depend on time.

Matching data to the model output requires defining a cost functional, which is not trivial in the case where data depend on both space and time. The most natural choice would be the following least-squares functional:

$$F_{LS}[D] = \frac{\sum_{i=1}^{N} \sum_{m=1}^{M} \left[T(x_i, t_m) - T_{\text{eff}}(x_i, t_m, D) \right]^2}{\sum_{i=1}^{N} \sum_{m=1}^{M} \left[T(x_i, t_m) - \overline{T}(x_i) \right]^2},$$
(3)

where $\overline{T}(x_i) = (1/M) \sum_{m=1}^M T(x_i, t_m)$, which provides for a better normalization. Numerical experiments reveal, however, that the effective diffusivity reconstructed with this functional fails to capture the growth of potatoes. Namely, $D_{\rm eff}$ remains in the neighborhood of the soil diffusivity $D_{\rm s}$ during most of the growing season, see Fig. 6.

As was discussed in the previous Section, phase shift of the temperature signal due to potatoes appears to be rather significant. The following correlation-based functional is aimed at equalizing phase shifts:

$$F_{\rm C}[D] = \frac{\sum_{i=1}^{N} \left[C_i(T) - C_i(T_{\rm eff}) \right]^2}{\sum_{i=1}^{N} \left[C_i(T) \right]^2},\tag{4}$$

where $C_i(T)$ measures by how much the data or the effective model are shifted with respect to the background temperature signal, i.e.,

$$C_{i}(T) = \frac{\sum_{m=1}^{M} \left[T(x_{i}, t_{m}) - \overline{T}(x_{i}) \right] \left[T_{b}(x_{i}, t_{m}) - \overline{T}_{b}(x_{i}) \right]}{\sigma_{i}(T)\sigma_{i}(T_{b})},$$

$$\sigma_{i}(T) = \left[\sum_{m=1}^{M} \left| T(x_{i}, t_{m}) - \overline{T}(x_{i}) \right|^{2} \right]^{1/2}.$$
(5)

Figure 6 demonstrates the shapes of F_{LS} and F_{C} functionals at different days of the simulated growth season. It is clear that F_{C} is both more sensitive to the changes in potatoes and has a "deeper" minimum that is easier to detect.

Figure 7 shows the evolution of $D_{\rm eff}$ throughout the season, where the effective diffusivity has been determined by finding the global minima of $F_{\rm LS}[D]$ and $F_{\rm C}[D]$ (solid lines). To this end the effective model has been run for a range of 100 values of the diffusivity D uniformly distributed between $D_{\rm p}$ and $D_{\rm s}$, and the corresponding temperature data were saved and reused to produce functionals $F_{\rm LS/C}$ for each day of the season. There exist much more efficient reduced-order approaches to this kind of problems, e.g. [9], which are not discussed in the present proof of the principle study.

The functional F_C is clearly not unimodal and its second minimum happens within the interval of interest. Moreover, sometimes the minimum that corresponds to physically acceptable effective diffusivity is not a global minimum. Thus, finding a global minimum is not necessarily a good strategy in effective inversion. In Fig. 7, $D_{\rm eff}(t)$ at the global minimum is shown with a solid line. While it features an almost linear decline with time after day 30, prior to that it demonstrates sporadic growth, which is caused by the right minimum in Fig. 6 being somewhat deeper than the left one. Fortunately, in the present case it is quite easy to decide which of the two minima to choose by incorporating the *a priori* dynamic information that potatoes grow rather than become smaller with time. This means that whenever $D_{\rm eff}(t)$ tends to increase one should choose the second minimum

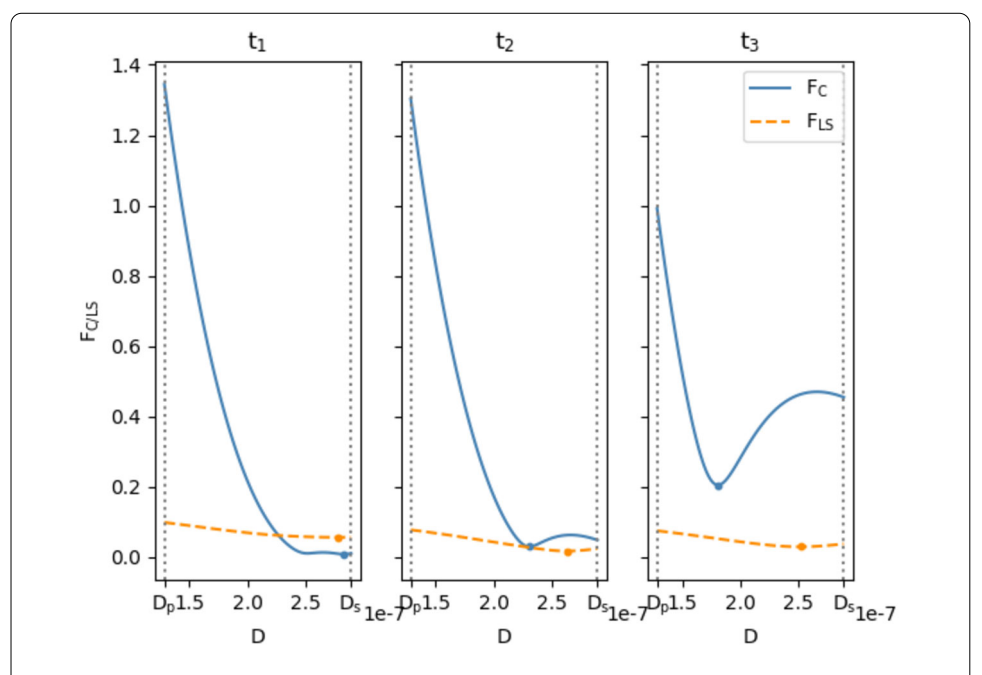


Figure 6 Shapes of least-squares and correlation-based cost functionals based on 24-hour data sampled at hourly intervals at three days during the growth season ($t_1 = 3$, $t_2 = 35$, and $t_3 = 70$ days). Actual configuration consists of 12 circular growing "potatoes" randomly placed within the boundaries of the effective domain

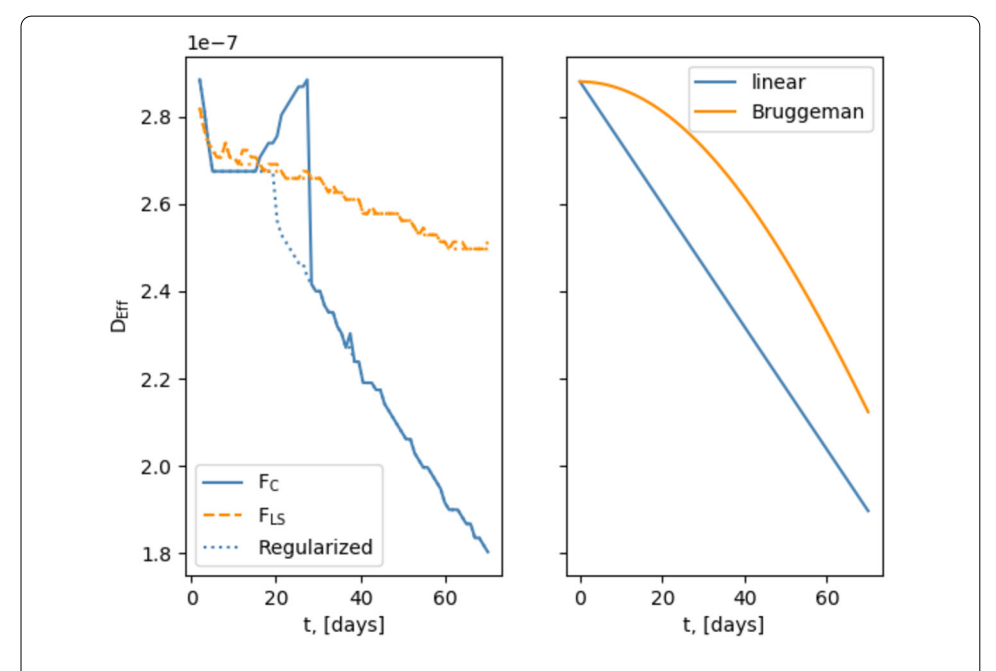


Figure 7 Left: effective diffusivity $D_{\rm eff}(t)$ as a function of time in days during the growth season reconstructed by minimizing $F_{\rm LS}$ and $F_{\rm C}$ cost functionals over 24 hour intervals. Dotted lines show the regularized results. Right: analytical approximations based on the mixing formulas (8) and (9)

of the functional. In cases where the second minimum can not be detected, the value of $D_{\rm eff}(t)$ obtained at the previous day is retained. The result of this simple regularization strategy is shown in Fig. 7 with dotted lines.

Computing an effective constitutive parameter for a medium consisting of inclusions in a homogeneous host material is the subject of effective medium theory [11]. According to the steady-state Bruggeman theory the effective parameter depends on the volume fraction of inclusions. In the present two-dimensional case $D_{\rm eff}$ is expected to satisfy the following equation:

$$\tilde{A}_{p} \frac{D_{p} - D_{eff}}{D_{p} + D_{eff}} + \left(1 - \tilde{A}_{p}\right) \frac{D_{s} - D_{eff}}{D_{s} + D_{eff}} = 0,$$
(6)

where $\tilde{A}_{\rm p}(t) = A_{\rm p}(t)/A_{\rm eff}$, $\tilde{A}_{\rm p}(0) = 0$, $\tilde{A}_{\rm p}(t=70\,{\rm days}) = 0.382$ is the relative area of inclusions (potatoes) at day t and $A_{\rm eff} = 0.355\,{\rm m}^2$ is the area of the effective domain depicted in Fig. 5 (right). Under the natural assumption that $D_{\rm p}$, $D_{\rm s}$, $D_{\rm eff}$, and $\tilde{A}_{\rm p}$ are all positive the Bruggeman equation simplifies to

$$D_{\text{eff}}^2 - (2\tilde{A}_p - 1)(D_p - D_s)D_{\text{eff}} - D_p D_s = 0, \tag{7}$$

and admits the explicit solution:

$$D_{\text{eff}}(t) = \frac{1}{2} \left[(2\tilde{A}_{p}(t) - 1)(D_{p} - D_{s}) + \sqrt{(2\tilde{A}_{p}(t) - 1)^{2}(D_{p} - D_{s})^{2} + 4D_{s}D_{p}} \right]. \tag{8}$$

Figure 7 (right) shows that neither the least-squares nor the correlation-based functional produce $D_{\rm eff}$ that follows Bruggeman's law. The fact that $F_{\rm LS}[D]$ shows a lack of decrease in effective diffusivity with the growth of low-diffusivity inclusions in a high-diffusivity host medium is difficult to explain. Of course, the present configuration, characterized by small particle numbers in a finite and relatively small host domain, makes the applicability of effective medium theories highly questionable. In addition, the 24-hour time interval used in the daily minimization problems may be too short to capture the instantaneous properties of growing tubers and the heat transfer on a given day is influenced by the state of tubers and temperature distribution of the previous day.

The correlation-based functional $F_C[D]$ is, on the other hand, much more sensitive to the tuber size and leads to $D_{\text{eff}}^C(t)$ which is well approximated by the following simple linear mixing formula:

$$D_{\text{eff}}^{C}(t) = D_{\text{p}}\sqrt{\tilde{A}_{\text{p}}(t)} + D_{\text{s}}\left(1 - \sqrt{\tilde{A}_{\text{p}}(t)}\right). \tag{9}$$

Notice that the effective diffusivity is determined here by the relative "diameter" $\sqrt{\tilde{A}_p}$ of the potato domain rather than its relative area \tilde{A}_p . Subsequently, this expression can be used to infer the temporal evolution of $\tilde{A}_p(t)$ from $D_{\text{eff}}(t)$ as

$$\tilde{A}_{p}(t) = \left(\frac{D_{\text{eff}}^{C}(t) - D_{s}}{D_{p} - D_{s}}\right)^{2}.$$
(10)

5 Conclusions

Numerical experiments presented in this paper show that diurnal temperature waves may be used to visualize the growth of tubers, such as potatoes. To this end a sparse array of thermal sensors can be placed below the seed tubers at the time of planting and monitored throughout the season at hourly intervals. While the amplitude of relevant temperature variations is expected to be in the order of 0.1 degrees, an imaging algorithm is proposed that relies on the relative synchronization rather than absolute precision of sensors. An effective inversion algorithm describing growing tubers in terms of effective time-dependent diffusivity has been demonstrated as well. The effective diffusivity reconstructed from time-domain data depends on the choice of the cost functional. It has been shown that neither the least-squares nor the correlation-based functional leads to an effective diffusivity that follows Bruggeman's mixing formula. The correlation-based functional is more sensitive to the changes in the relative volume of potatoes, but requires additional regularization due to the presence of the second minimum. A simple linear mixing formula is proposed that allows to reconstruct the relative volume of potatoes from the effective diffusivity obtained by minimizing the correlation-based cost functional.

While we did not perform targeted simulations with artificial additive noise, the "noise" in our numerical experiments was still introduced by the numerical truncation errors and mesh changes in the FEM numerical solver used to produce synthetic data. It appears that the proposed imaging algorithm is robust against such noise since, by construction, it does not involve any ill-conditioned operations on the data. The images become noisy only when the signal from the tubers is very small as in Fig. 4 (bottom, left). The effective inversion algorithm, on the other hand, requires finding the minimum of a relatively smooth function, which is a potentially ill-conditioned mathematical procedure, generally sensitive to noise in the data. The usual least-squares loss (cost) functional appears to have a unique minimum but is smooth around the minimum point, making it more sensitive to noise. An alternative, correlation-type loss functional has a more pronounced minimum, i.e., is less sensitive to noise, but suffers from the presence of the second (false) minimum at the early growth stage (small tubers).

The practical applicability of the proposed imaging algorithm depends on the feasibility of measuring the two-dimensional temperature distribution on the soil surface. We suggest that these measurements are performed with a thermistor network [12], which requires a limited number of connecting wires, little electric power, and is easy to control. For the effective inversion algorithm, a simpler vertically positioned linear array of thermal sensors can be employed [13]. With both sensor types, it is crucial to account for the factory differences in the temperature-resistance characteristics of thermistors. This calibration is usually performed in a well-controlled spatially uniform thermal bath. As our simulations indicate, the background temperature readings required by both the imaging and the effective inversion algorithms can be obtained from the sensors that are located some distance away from the tubers.

Author contributions

NB posed the problem, supervised the research, performed 3D simulations, implemented the imaging algorithm, MB performed 2D simulations, implemented the effective inversion algorithm, performed numerical experiments. All authors read and approved the final manuscript.

Funding information

This research was performed at TU Delft and did not involve any external or commercial funding.

Data availability

This paper does not make use of any experimental data, a mix of proprietry (COMSOL) and open-source (Python, NumPy, FEniCS) software was used to perform simulations.

Declarations

Competing interests

The authors declare no competing interests.

Author details

¹ Numerical Analysis, Delft Institute of Applied Mathematics, Faculty of Electrical Engineering, Mathematics and Computer Science, Delft University of Technology, Mekelweg 4, 2628 CD Delft, The Netherlands. ² Present address: TOPdesk Nederland BV, Westlandseweg 40, 2624 AD Delft, The Netherlands.

Received: 15 March 2024 Accepted: 1 August 2025 Published online: 18 August 2025

References

- Konstantinovic M, Wöckel S, Lammers PS, Sachs J, Martinov M. Detection of root biomass using ultra wideband radar

 an approach to potato nest positioning. Agric Eng Int. 2007;9:06003.
- 2. Lei S, Daniels JL, Bian Z, Wainaina N. Improved soil temperature modeling. Environ Earth Sci. 2011;62:1123–30.
- 3. Tabatabaei N, Mandelis A. Thermal-wave radar: a novel subsurface imaging modality with extended depth-resolution dynamic range. Rev Sci Instrum. 2009;80:034902.
- Ghali VS, Mulaveesala R. Comparative data processing approaches for thermal wave imaging techniques for non-destructive testing. Sens Imaging. 2011;12:15–33.
- 5. Jong van Lier Qd, Durigon A. Soil thermal diffusivity estimated from data of soil temperature and single soil component properties. Rev Bras Ciênc Solo. 2013;37:106–12.
- Mimouni T, Lei L, Laloui L. Estimating soil thermal diffusivity with interference analyses. Acta Geotech. 2015;10:197–208.
- 7. Magee TRA, Bransburg T. Measurement of thermal diffusivity of potato, malt bread and wheat flour. J Food Eng. 1995:25:223–32.
- Budko N, van den Berg P. Characterization of a two-dimensional subsurface object with an effective scattering model. IEEE Trans Geosci Remote Sens. 1999;37:2585–96.
- 9. Budko NV, Remis RF. Electromagnetic inversion using a reduced-order three-dimensional homogeneous model. Inverse Probl. 2004;20:S17–26.
- 10. Raghunathan SB, Budko NV. Effective permittivity of finite inhomogeneous objects. Phys Rev B. 2010;81:054206.
- 11. Choy TC. Effective medium theory: principles and application. Oxford: Clarendon Press; 1999.
- 12. Schäfer T, Schubert M, Hampel U. Temperature grid sensor for the measurement of spatial temperature distributions at object surfaces. Sensors. 2013;13:1593–602.
- 13. Wuest SB. An array for measuring detailed soil temperature profiles. Soil Sci Soc Am J. 2012;77:427–31.

Publisher's note

Springer Nature remains neutral with regard to jurisdictional claims in published maps and institutional affiliations.

Submit your manuscript to a SpringerOpen journal and benefit from:

- ► Convenient online submission
- ► Rigorous peer review
- ▶ Open access: articles freely available online
- ► High visibility within the field
- ► Retaining the copyright to your article

Submit your next manuscript at ▶ springeropen.com